

# AN UNSUPERVISED MACHINE LEARNING APPROACH FOR GROUND MOTION CLUSTERING AND SELECTION

**R. Bailey Bond<sup>a</sup>, Pu Ren<sup>a</sup>, Jerome F. Hajjar<sup>a,1</sup> and Hao Sun<sup>b,1</sup>**

<sup>a</sup> Department of Civil and Environmental Engineering, Northeastern University, Boston, MA 02115, USA

<sup>b</sup> Gaoling School of Artificial Intelligence, Renmin University of China, Beijing, 100872, China

Clustering analysis of sequence data continues to address many applications in engineering design, aided with the rapid growth of machine learning in applied science. This paper presents an unsupervised machine learning algorithm to extract defining characteristics of earthquake ground-motion records, also called latent features, to aid in ground-motion clustering and selection. In this context, a latent feature is a low dimensional machine-discovered spectral characteristic learned through nonlinear relationships of a neural network autoencoder. Clustering can be performed on the latent features and used to select a representative archetypal subgroup from a large ground-motion suite. The objective of efficient ground-motion selection is to choose records representative of what the structure will probabilistically experience in its lifetime. Three examples are presented to validate this approach, including a synthetic spectral dataset and spectra from field recorded ground-motion records. Deep embedding clustering of ground motion spectra improves on the results of static feature extraction, utilizing characteristics that represent the sparse spectral content of ground motions.

## INTRODUCTION

Feature engineering is critical in representation learning and is used in many domains with applications like stock price forecasting (Long et al., 2019), neurological diagnosis (Wang et al., 2019), and acoustic scene classification (Pham et al., 2020). Unsupervised machine

---

<sup>1</sup> Corresponding Authors

learning (ML) is a tool in artificial intelligence (AI) used to deduce the natural structure within a dataset lacking target labels. Unsupervised feature extraction can greatly enhance the characterization of sequence data with complex frequency content and can be used to select a subgroup from a large dataset. One aim of feature engineering is to use domain knowledge to identify key features of unlabeled data, effectively compressing the dimensionality of the data into its most important components (Bengio et al., 2013). A few existing methods of feature extraction include principal component analysis (PCA) (Pearson, 1901), local linear embedding (Rowels and Saul, 2000), and autoencoders (Kramer, 1991). An autoencoder employs the nonlinear parameter discovery of a neural network (NN) to identify relationships which can outperform the linear dependencies of other existing methods (Kramer, 1991). Furthermore, modifications to the typical autoencoder architecture have been studied to accomplish specific tasks (Baldi, 2012).

The deep embedded clustering scheme is adopted here which is defined by a parameterized nonlinear mapping from the data space to a lower dimensional feature space, where a clustering objective is then optimized (Xie et al., 2016). The *k*-means approach is one of the most popular clustering algorithms chosen for ML-based applications (Coates and Ng, 2012). With the low dimensional feature space, *k*-means clustering can be performed to identify groups of similar data. A selection from each cluster can be added to an archetypal subgroup, representative of the complete original dataset.

This selection process can be useful in the context of ground-motion selection. High fidelity earthquake loading presents a large computational expense for structural analysis such as finite element modeling (FEM) and structural metamodeling. The suite of ground motions selected for loading when conducting nonlinear response analysis for civil structures can have a large impact on the predicted structural behavior (Whittaker et al., 2012). An optimal selection will include as few ground motions as possible while still expressing all representative events the structure will probabilistically experience in its lifetime (Katsanos et al., 2010). The current building codes provide some guidance for ground-motion selection but do not define the use of specific methods. Chapter 21 of ASCE 7, “Site-Specific Ground-Motion Procedures for Seismic Design,” states “At least five recorded or simulated horizontal ground-motion acceleration time histories shall be selected from events having magnitudes and fault distances that are consistent with those that control the [maximum considered earthquake]” (ASCE 7-16

2000). Consequently, there are multiple methods of selection used in practice with some divergences to the final structural response and ultimate design.

Classical methods of selection include clustering based on physical attributes such as magnitude, peak ground acceleration (PGA), or other intensity measurements (IMs) (Baker and Cornell, 2006; Ding et al., 2020; Rehman et al., 2014). Although these measurements might possess connections to dynamical properties of earthquakes, this categorical approach might fail to include critical attributes or hidden characteristics resulting in a less representative ground-motion selection. It is noted that even in the earliest studies on strong ground motions, single IMs cannot reliably predict the damage potential of such a complex process (Housner and Jennings, 1982). More novel methods of classifying ground motion features which aim at characterizing the spectral frequency content have been proposed (Yaghmaei-Sabegh, 2017). In this method, *k*-means clustering and self-organizing map (SOM) network algorithms are used to reveal six descriptive features. However, these features still rely on human engineered parameters that do not incorporate the entire spectral behavior. The most current existing method of ground-motion selection and modification is the conditional mean spectra (CMS) where a statistical analysis of the spectrum conditioned on a period of interest reveals a hazard-consistent design spectrum (Baker, 2011; Lin et al., 2013). CMS leads the designer to a more realistic spectrum compared to the Uniform Hazard Spectrum (UHS) provided by building codes. Spectral matching (shape matching) can then be performed to match the hazard-consistent design spectrum at all spectral periods, specifically the period of interest, by modifying the frequency content of the time-series (Hancock et al., 2006; Iervolino et al., 2010). However, there has been evidence advising against spectral matching and excessive scaling, favoring the use of measured ground motions (Grigoriu, 2011; Naeim et al., 2004). In some cases, the distortion resulting from scaling real records to target levels or modifying the frequency content and phasing of real records to match a smooth target spectrum can make these records more aggressive than real/un-scaled records with spectra naturally at a similar target level (Bazzurro and Luco, 2005). Additionally, the CMS method only provides a target spectrum. For example, if a spectrum matches the CMS, then it is viewed as a valid selection. This selection might be ignoring critical spectral characteristics of another spectrum that also matches the CMS but was not chosen. Nevertheless, the main advantages to these methods is to reduce the number of ground-motion records required for engineering analysis and provide probabilistically relevant spectra to the site of interest.

ML is becoming increasingly common in earthquake engineering and seismological applications (Kong et al., 2019). To address the lack of full representation (e.g., the consideration of all available spectra relevant to a site of interest) in traditional and current ground motion selection methods, ML can be used to encode full spectra into a primary set of characteristics to diversify the selection process and reduce the reliance on human engineered features. To this end, an unsupervised ML method to cluster spectra and ultimately select ground motions from a group of available ground-motions is presented here. In this process, assumptions of statistical distributions of ground-motion characteristics or other common ground-motion selection measures are left out. The following explains a process of spectral selection by applying a general sequence clustering problem. It is hypothesized that the key features of the spectra will be learned by the deep embedding framework.

In this approach, a comprehensive suite of recorded ground motions is selected from the Pacific Earthquake Engineering Research Center (PEER) NGA West 2 Database. A fully connected NN autoencoder was developed to uncover latent features, or hidden characteristics, of the ground-motion suite, that encapsulate low dimensional machine discovered spectral characteristics. Two examples consisting of a synthetic ground-motion dataset and pre-grouped field measured dataset are presented to validate the deep embedding clustering framework.

Due to the nature of unsupervised learning, the latent features used in analysis are discovered through black box learning, and cannot be fully interpreted by the user, but can yield a deeper more accurate categorization of the ground motion spectra compared to known static measurements. It will be shown, the discovered latent features possess correlations to the traditional ground-motion intensity measures, giving the user a relative idea of the latent feature's interpretability.

## **METHODOLOGY**

This section outlines the formulation of the deep embedding unsupervised ML clustering approach for ground-motion selection. The autoencoder can be trained on a suite of ground-motion spectra from which a selection is desired, resulting in a user defined number of latent features. Each set of latent features correlates to an input spectrum. A clustering algorithm is used to group the spectra on the discovered features and a representative selection is made from each cluster.

## Data Selection and Scaling

For NN training, a rich inclusive dataset is desirable. From testing different scaling methods, the authors hypothesize that the autoencoder's ability to learn effectively correlates with the trends and shape of the spectra. With a large variance in the magnitude of unnormalized spectra, the proposed autoencoder is thought to parameterize the magnitude over the divergence. To alleviate this issue, the data was normalized on the smallest period (e.g.,  $T = 0.05$ ) to optimize performance by emphasizing the divergence between sequences while preserving the spectral shape. Because it is desired to select representative ground motions from all data available, the spectra were not split into a testing set and training set, rather, all data was used for training. This approach is common for unsupervised machine learning applications with data lacking labels, requiring other means of validation. Additionally, spectral series were used over time-series ground accelerations due to their significant influence on the structural response of civil structures and broad use in earthquake engineering analysis and design.

The presented framework can be applied to any group of ground motions available to a user of the method. For example, a probabilistic seismic hazard analysis (PSHA) provides a user with many ground-motion parameters statistically significant to a user's site of interest. Training the presented model on a group of ground motions that match these parameters could give the user a representative selection from the relevant ground motions. Furthermore, a group of hazard-consistent spectra, conditioned at a period of interest, could also be used as an initial group to train the autoencoder for clustering and selection. To show broad use cases, the manuscript only delineates general examples, which highlight the quality and characteristics of the presented latent space, and the ability to select ground motions which are sufficiently spread in this space.

## Autoencoder Implementation and Training

The proposed autoencoder network architecture is illustrated in Figure 1. Similar to nonlinear principal component analysis, autoencoders were developed to uncover latent features, or lower dimensionality encodings for unlabeled data (Kramer, 1991). Stochastic gradient descent (SGD) via backpropagation on a traditional mean square error (MSE) objective function learns the mapping, which is parameterized with  $\theta$  and  $\phi$  by a deep NN encoder and

decoder (e.g.,  $g_\phi(x)$  and  $f_\theta(x)$  respectively). The formal objective function for  $n$  observations of input sequence  $\mathbf{x}^{(i)}$  is shown as follows

$$\mathcal{L}(\theta, \phi) = \frac{1}{n} \sum_{i=1}^n \left( \mathbf{x}^{(i)} - f_\theta \left( g_\phi \left( \mathbf{x}^{(i)} \right) \right) \right)^2. \quad (1)$$

where  $\theta = \{\mathbf{W}_\theta, \mathbf{b}_\theta\}$  and  $\phi = \{\mathbf{W}_\phi, \mathbf{b}_\phi\}$ . The autoencoder compresses the input to latent representation using fully connected nodes and then reconstructs the original signal and minimizes the reconstruction error. For more information pertaining to autoencoders, the authors defer to (Baldi, 2012).

To enhance performance of the autoencoder, a residual connection from the first layer in deconstruction to the last layer in reconstruction has been found to guide the latent space to more optimal result, while improving the reconstruction. A tensor concatenation was performed on the copied parameters from the encoder's hidden layer with the feature map of the last decoder's hidden layer. Using a residual connection with the concatenation operation allows a congruent flow of information from the latent space and the residual connection. This type of construction allows subsequent hidden layers the ability to re-use prior feature representations while providing better gradient propagation which is accomplished with implicit deep supervision (Lee et al., 1998). The benefits of the residual connection are two-fold. Firstly, the residual connection leads to a significantly better reconstruction of the spectra. The reconstruction of the spectra is an important part of the validation of the performance of the autoencoder. Although the latent representation will be utilized for clustering and selection, without sufficiently low reconstruction error, the latent space should not be trusted as an accurate representation. Secondly, the latent space possesses more interpretable organization of recognizable features with respect to the static IMs. An ablation study that shows the reconstruction and organization of the latent space without the residual connection is presented for the last real-world example to further examine the effects of the residual connection.

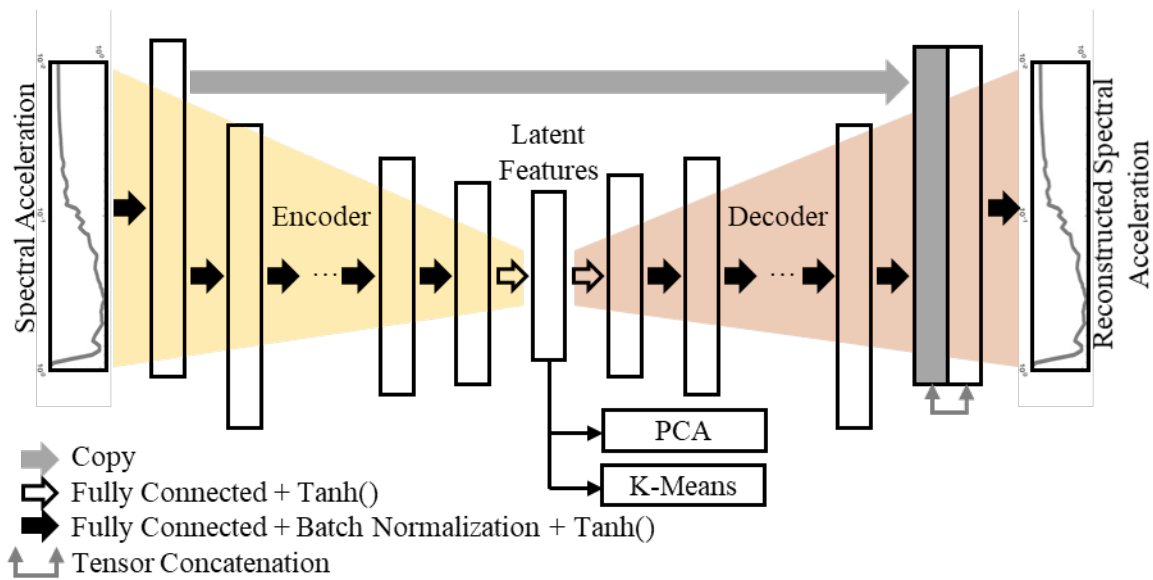


Figure 1: Network architecture.

A parametric analysis was conducted to optimize the autoencoder's hyperparameters. The number of fully connected hidden layers and the number of nodes in the hidden layers were generally reduced from the previous dimension by multiples of 4 until reduction approached the user defined number of latent features. The original dimension of the spectra was 996 and 3981 for the synthetic spectra and field measured spectra, respectively. Consequently, the hidden layer for the encoder was of the form 996-512-128-32-4 and 3981-2048-512-128-32-12 for the synthetic data and field measured data, respectively. The decoder possesses the same structure in reverse. The hyperbolic tangent activation function (e.g., tanh) was chosen to capture the nonlinear features of the spectral data and was shown to outperform the rectified linear unit (ReLU) activation function in testing. Batch normalization layers are used between hidden layers to obtain a steady distribution of activation values during training. The minibatch size is set to 50 for the synthetic dataset and 124 for the field measured data. The weight decay parameter is set to  $1e-6$ , and the starting learning rate is set to  $1e-3$ , with a learning rate decay period of 200 epochs and a multiplicative factor of 0.9. All the above hyperparameters are held constant across all datasets and were found to suitably minimize the reconstruction error in all cases (e.g., see Figure 2). Data specific tuning of these hyperparameters might improve performance on each dataset, but idealistic parameter tuning is impractical for real world implementation.

The presented method can be used with existing methods to increase representation of the selection from an initial group but would require re-training of the Autoencoder and re-

selection of ground motions for each structure and each site of interest. Other architectures and training methods including additional residual connections, convolutional layers, transfer learning, and variational autoencoders will be explored in our future work. Additionally, future work will include different clustering techniques to avoid the drawbacks of the  $k$ -means clustering method mentioned in the next section of this paper.

### Ground-Motion Clustering and Selection

Although the clustering method will influence the exact spectra chosen from the latent space, if clustering results in spectra that are sufficiently separated in the latent space, then the exact means of clustering is somewhat trivial. Clustering methods may be chosen by a user of the framework based on features of the latent space representations.

For clustering in this application, a standard Euclidean  $k$ -means clustering algorithm was chosen for its simplicity and interpretability. It is noted that the  $k$ -means clustering algorithm possesses some distinct features that might diminish its clustering performance for specific tasks, including a substantial dependence on initial conditions and clusters of varying sizes, densities, and shapes (Coates and Ng, 2012; Kodinariya and Makwana, 2013; Rehman et al., 2014). The spectra are assembled into  $k$  clusters utilizing the latent features as the observations. A set of observations  $(\mathbf{z}_1, \mathbf{z}_2, \dots, \mathbf{z}_n)$ , where each observation (e.g., a  $d$ -dimensional list of latent features) is partitioned into  $k$  clusters  $(C_1, C_2, \dots, C_k)$  to minimize the within-cluster sum of squares (WCSS). The formal objective function is shown below.

$$\arg \min_C \sum_{i=1}^k \sum_{x \in C_i} \|\mathbf{z} - \boldsymbol{\mu}_i\|^2 = \arg \min_C \sum_{i=1}^k |C_i| \text{Var } C_i \quad (2)$$

where the  $\boldsymbol{\mu}_i$  is the mean of observations in  $C_i$ . The first step is to define  $k$  centroids, choosing them as far away from each other as possible. Next, all remaining observations are associated to the nearest centroid with the smallest Euclidean distance. When all observations are assigned to a group,  $k$  new centroids are calculated and the next iteration is performed. The loop is performed until the centroids do not move to new locations (Kodinariya and Makwana, 2013).

The elbow method and silhouette score were both used to define the optimal number of clusters (Kodinariya and Makwana, 2013). The prior calculates the WCSS for different values of  $k$ , choosing the number of clusters where the distortion first starts to converge, visible as an



elbow when plotted. A silhouette value ranges from +1 and -1, where a higher value indicates higher cohesion among the clusters. The silhouette value, Eqn. 3, is found by comparing a measure of similarity of the point  $i$  to its own cluster,  $\mathbf{a}(i)$  (Eqn. 4), and the measure of dissimilarity,  $\mathbf{b}(i)$  (Eqn. 5), where  $N_i$  is the number of observations belonging to cluster  $i$  and  $d(i, j)$  is the distance between observations  $i$  and  $j$  in the cluster  $C_i$ . For practical applications, the number of clusters can be selected contingent on the desired number of spectra for structural analysis and influenced by standards or the available computing power. For most cases, trends display that the fewer clusters chosen leads to higher cohesion between the clusters.

$$\mathbf{s}(i) = \frac{\mathbf{b}(i) - \mathbf{a}(i)}{\max\{\mathbf{a}(i), \mathbf{b}(i)\}}, \text{ if } C_i > 1 \quad (3)$$

where:

$$\mathbf{a}(i) = \frac{1}{N_i - 1} \sum_{j \in C_i, i \neq j} d(i, j) \quad (4)$$

and

$$\mathbf{b}(i) = \min_{i \neq j} \frac{1}{N_i} \sum_{j \in C_j} d(i, j) \quad (5)$$

For selection, centroids of the latent space clusters were defined and the spectra “closest” to the centroid was selected as the representative ground-motion for that group. Additionally, a linear orthogonal decomposition or PCA is performed on the latent space for cases with more than three latent features. 3D plots of the principal components provide a visual of the latent space representation, however, the latent features were used directly in the  $k$ -means clustering algorithm.

## EXAMPLES

This section illustrates the deep embedding clustering framework for three examples trained on different datasets, including synthetically derived and field measured spectral data. The first two examples show the effectiveness of the methodology and help substantiate the framework. The third example shows a real-world application a potential spectral latent space representation which resembles a wind range of spectral characteristics. The network training loss for each of the following examples are shown in Figure 2.

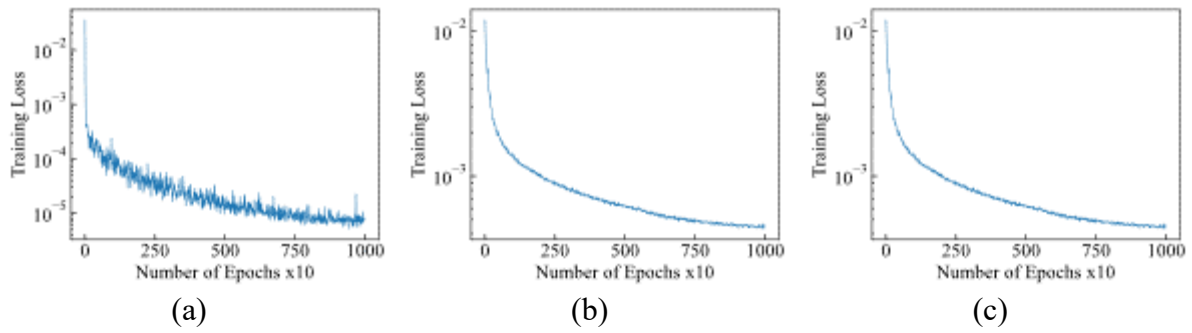


Figure 2: Network training loss for (a) the synthetic dataset; (b) the target magnitude PEER dataset; (c) the comprehensive PEER dataset;

### Clustering Sinusoidal Shape Time-Series

To assess the performance of the autoencoder and k-means clustering, 200 synthetically derived sinusoidal-shape time-series were tested on the framework. This example is a benchmark case that validates the application of an autoencoder to embed spectral features to a latent representation. The separation in the latent representation is shown to mimic the separation in the spectral shapes. This validates the idea that the resulting latent space has a correlation to the original spectra.

Four predefined clusters, consisting of 50 sequences each, were generated from sine waves with random phases and magnitudes. Each synthetic cluster possessed additional magnitude oscillations due to added noise and was converted to spectrum with periods ranging from 0.05 to 10 with at a 0.01 step size using the OpenSeismo toolbox in MATLAB R2020b (Papazafeiropoulos and Plevris, 2018). The four time-series clusters and spectral clusters can be clearly identified in Figure 3.

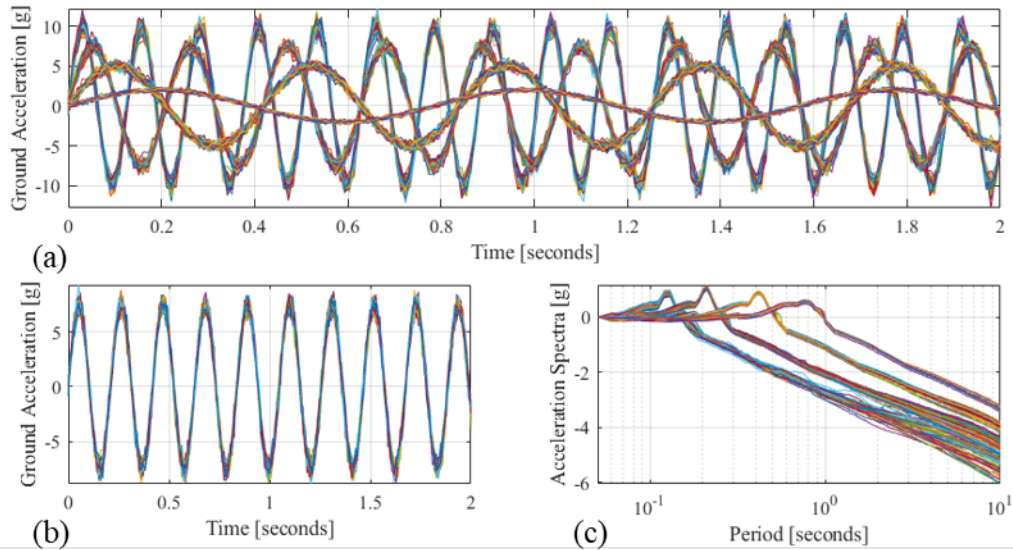


Figure 3: (a) Four clusters in time-series in the synthetic dataset; (b) zoom in view of one cluster of the synthetic dataset; (c) all spectral accelerations of the synthetic dataset.

The proposed framework was used to first discover four latent features of the 200 synthetic spectral series. A PCA is used to linearly combine the four latent features into three defining characteristics shown in Figure 4. With a predefinition of four clusters,  $k = 4$ , it is shown (see Figure 4) that with proper training, the framework can accurately identify ground truth clusters with 100% accuracy. The reconstruction of the spectra and the difference between the reconstruction and original spectral accelerations are shown in Figure 5. The spectra are separated into their discovered clusters in Figure 6.

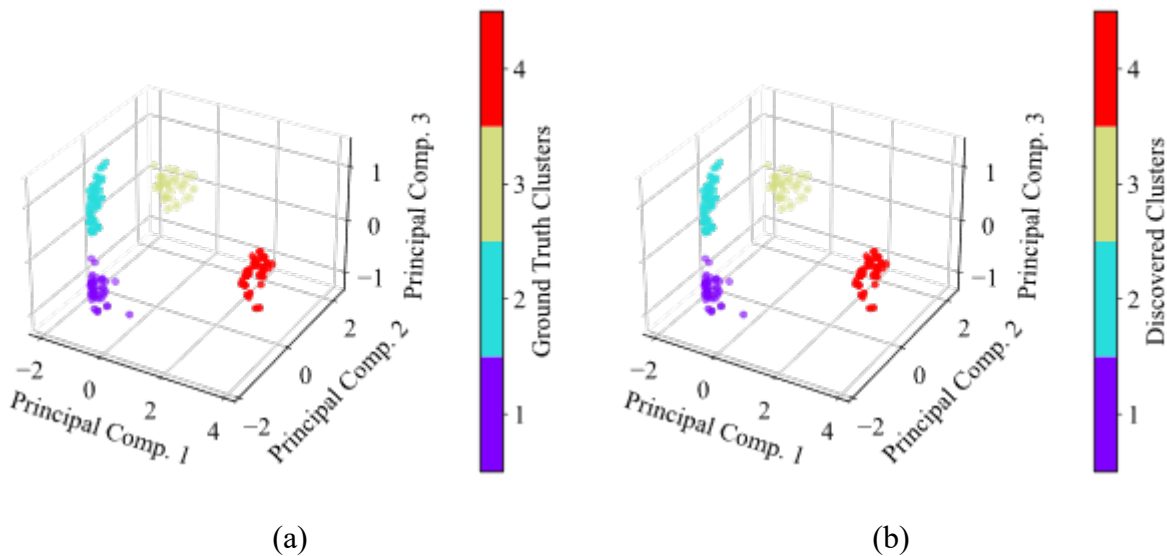


Figure 4: (a) Ground truth clusters latent space depicted with principal components; (b) discovered clusters latent space depicted with principal components.

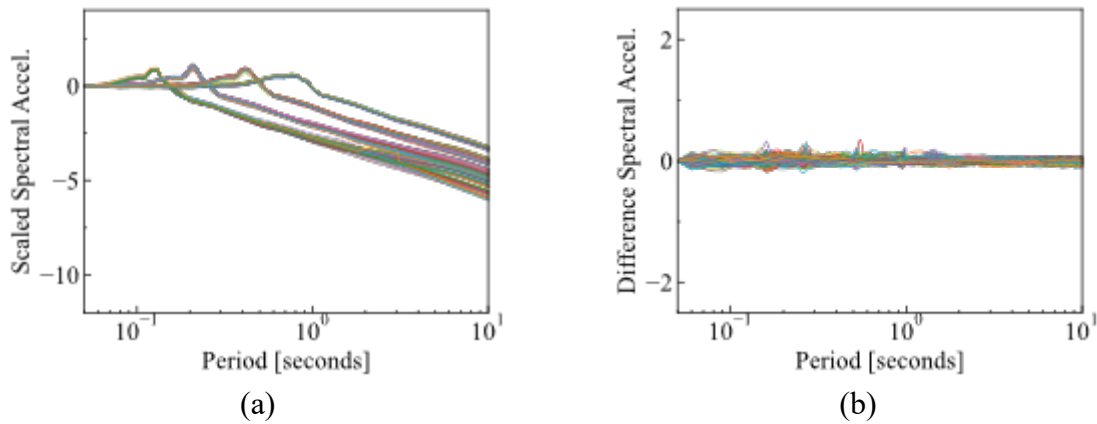


Figure 5: (a) Reconstructed spectral accelerations of synthetic dataset; (b) difference between reconstruction and original spectral accelerations.

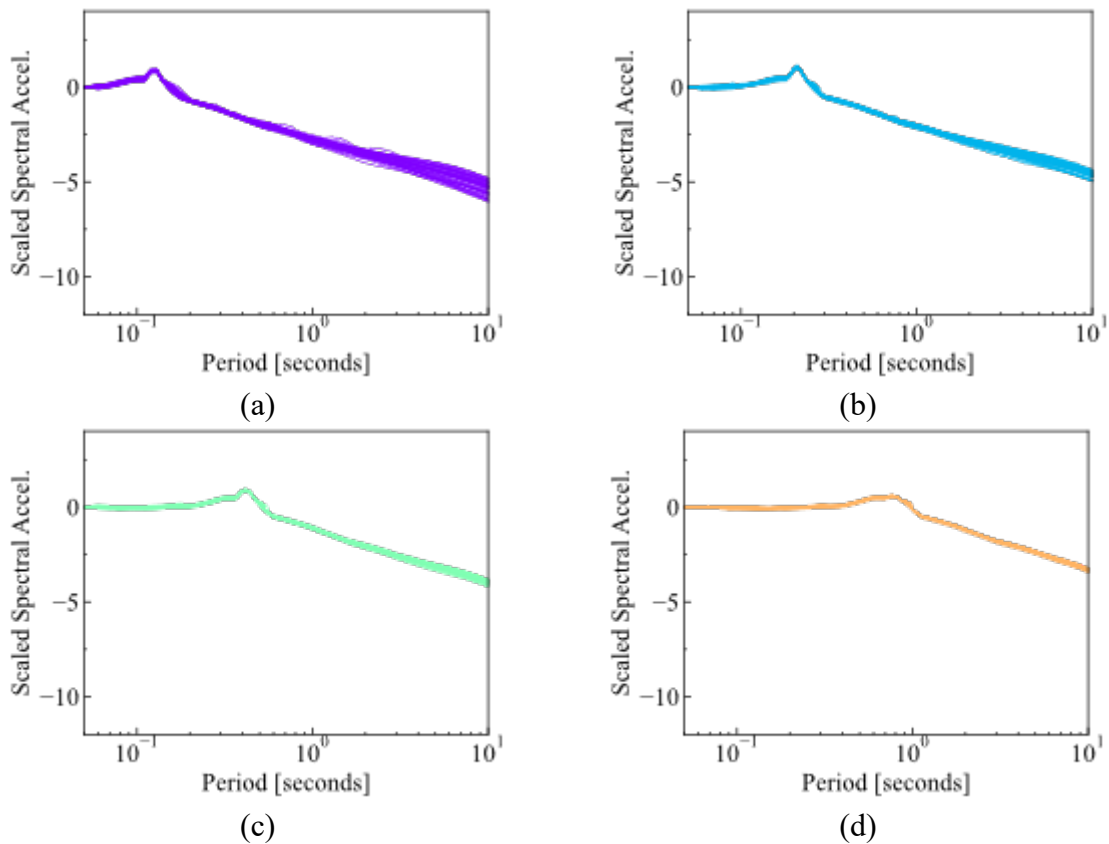


Figure 6: Deep embedding clustering of all synthetic spectral accelerations for (a) cluster 1; (b) cluster 2; (c) cluster 3; (d) cluster 4.

The silhouette score, a measure of cohesion between members of the same cluster, and the elbow method, a measure of distortion for different defined numbers of clusters, are combined to address the issue of predefining the optimal number of clusters (Kodinariya and Makwana, 2013). As shown in Figure 7, the optimal number of clusters using both methods is  $k = 4$ , where the modeling converges and adding another cluster does not yield a lower distortion in the elbow method or higher cohesion for the silhouette score.

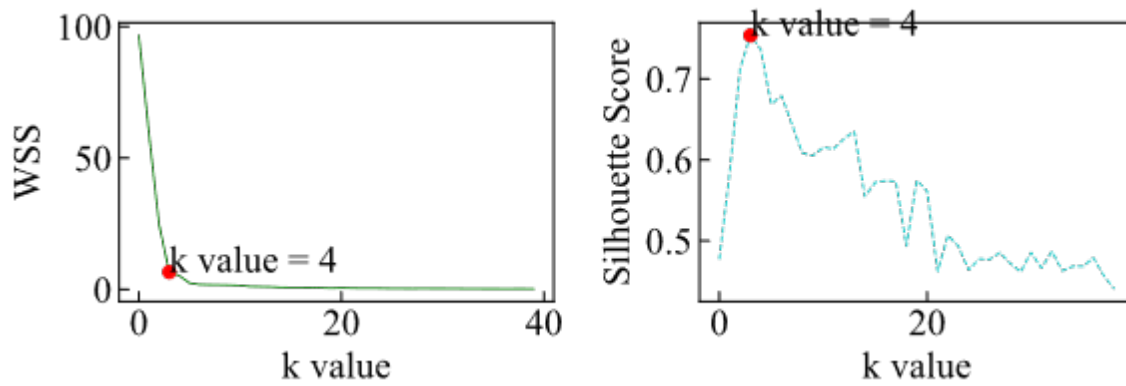


Figure 7: Identification of optimal number of clusters with the (a) elbow method and (b) the silhouette score.

### Clustering Ground-Motions Associated with Target Spectra

The second dataset comprised of ground-motion spectra, along with static attributes for each ground-motion, downloaded from the PEER NGA-West 2 Database (Ancheta et al., 2013). Spectra were placed in two groups; the first group, 1091 spectra, included M2 (magnitude 2) to M5 ground motions and the second group, 1157 spectra, comprised M7 to M9 ground motions. This decision was made to illustrate the relationship of the latent feature space with a well understood intensity measure (i.e., the earthquake magnitude). This example shows that a selection from each cluster results in a selection of different magnitude ground motions. However, because the latent space represents the entire spectral content, the records are not only based on magnitude.

Spectra downloaded from the PEER NGA-West 2 Database were originally in sequences with uneven increments of periods. To ensure the autoencoder was not over emphasizing one period value over another, and even step size of 0.01 was interpolated from the original data with a spline-based interpolation method. This resulted in a final sequence length of 3981 for each spectrum.

Twelve latent features were linearly decomposed to three principal components for visual purposes only. The twelve latent features were clustered into two groups using the  $k$ -means algorithm. The latent space representation, defined by the three principal components, colored by magnitude and the discovered clusters is displayed in Figure 8. The framework achieved a 99.1% accuracy for classifying high and low magnitude earthquakes from scaled spectral data alone.

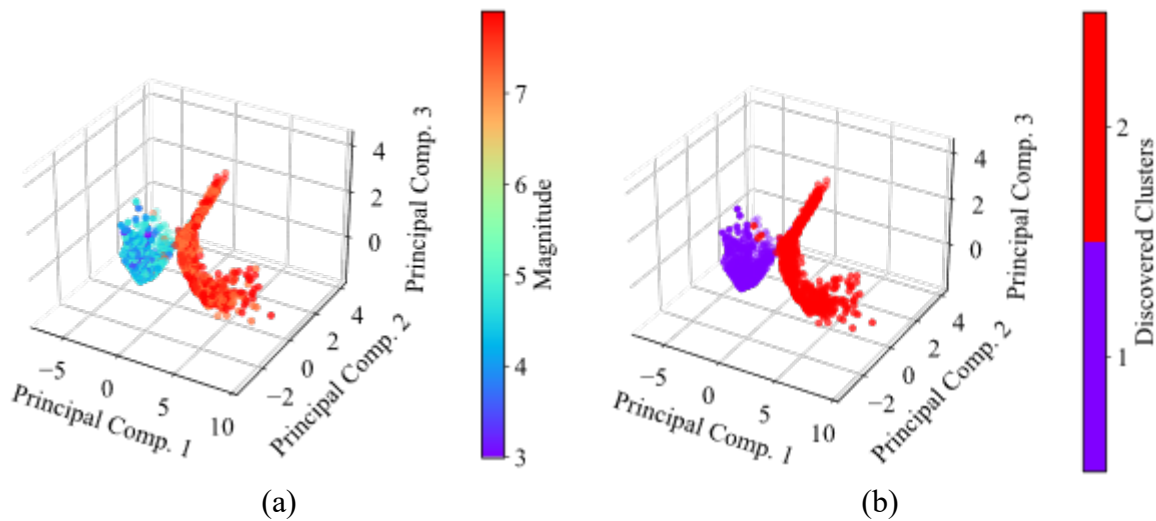
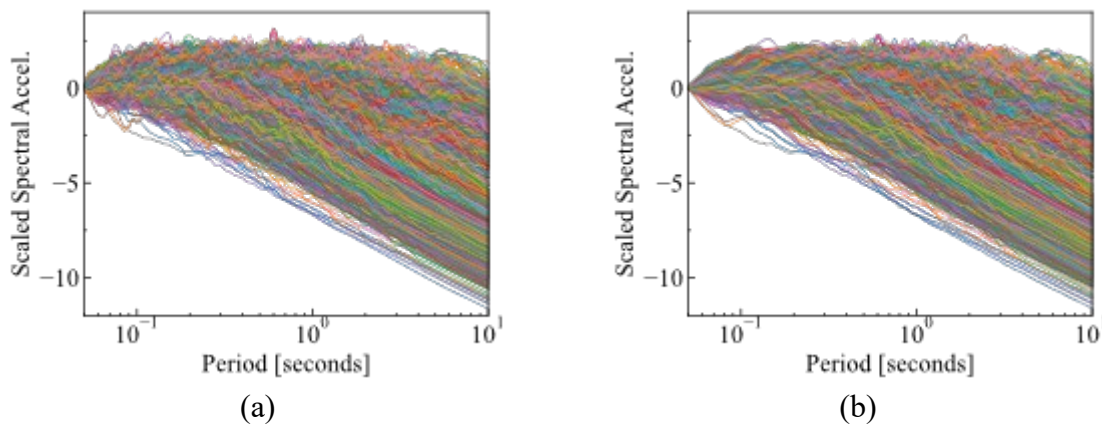


Figure 8: Latent space for ground motions associated with target magnitudes colored by (a) the magnitude and (b) the deep embedding discovered cluster.

This example reveals interpretability in the latent space; the discovered latent features for real ground-motion records show a correlation to the energy content of the spectra. The input, reconstruction, and reconstruction difference are shown in Figure 9, along with an example of five individual reconstructions. The results of the clustering are shown in Figure 10 for the scaled spectra where the colors correlate to their ground truth cluster (e.g., high or low magnitude). Figure 10 also shows the distribution of the two regions with high density clusters of spectra with overlapping spectra shapes from both groups. Additionally, the identified cluster centroids are shown to match a representative average of all spectra in the specified cluster at each period, termed the mean spectra, for each of the two cluster in Figure 11, adding to the confidence in the framework. The significance of the mean spectra shows that the typical spectral content at each period and for each cluster matches the spectra identified as the cluster's centroidal spectra.



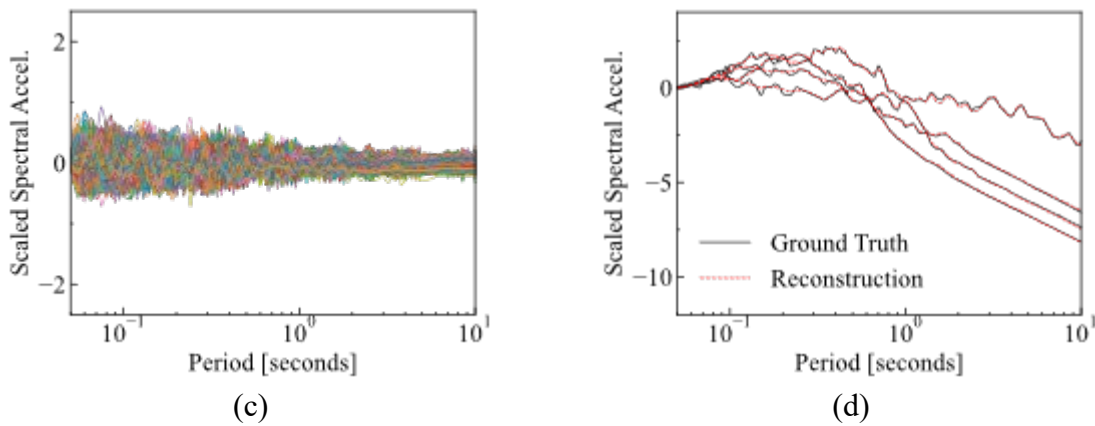


Figure 9: (a) Input spectra; (b) reconstructed spectra; (c) difference between input and reconstructed spectra; (d) reconstruction example.

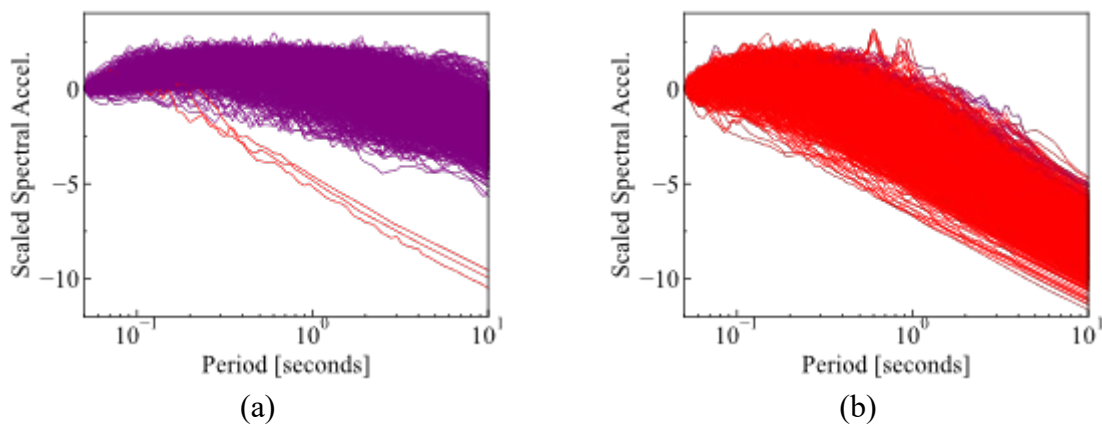


Figure 10: Deep embedding clustering of all magnitude grouped spectral accelerations for (a) cluster 1; (b) cluster 2;

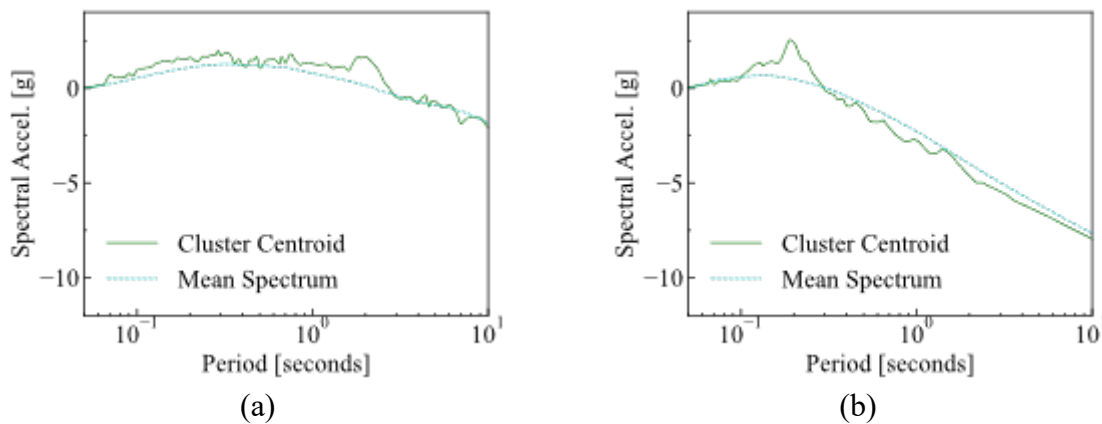


Figure 11: Mean cluster spectra compared to the spectrum closest to the centroid in the latent space for (a) cluster 1; (b) cluster 2;

### Clustering Earthquake Spectra for Ground-Motion Selection

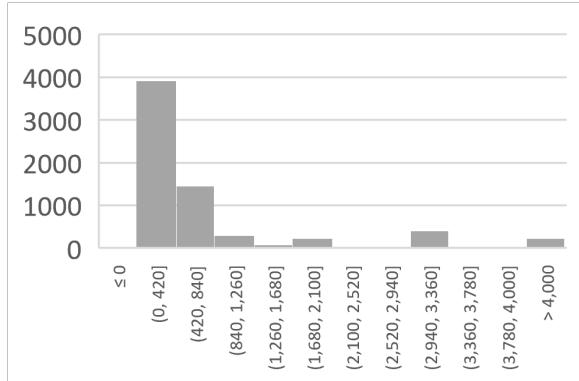
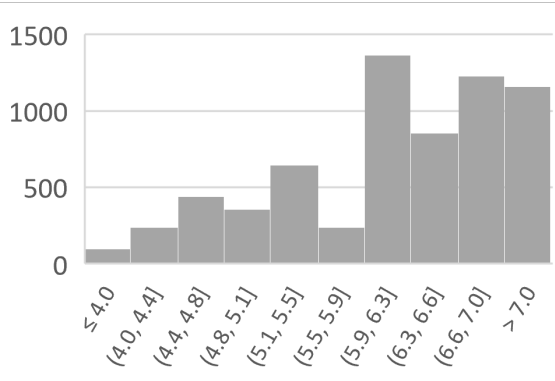
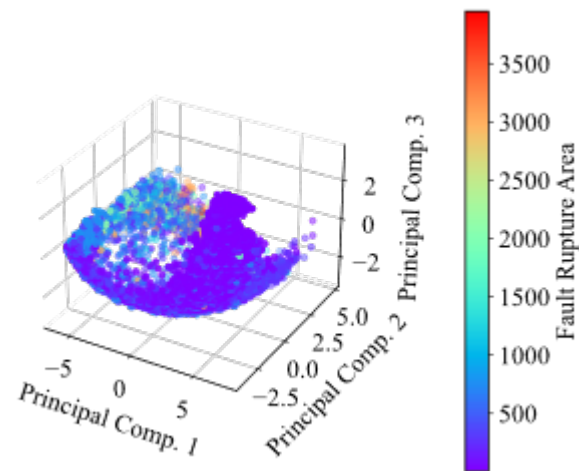
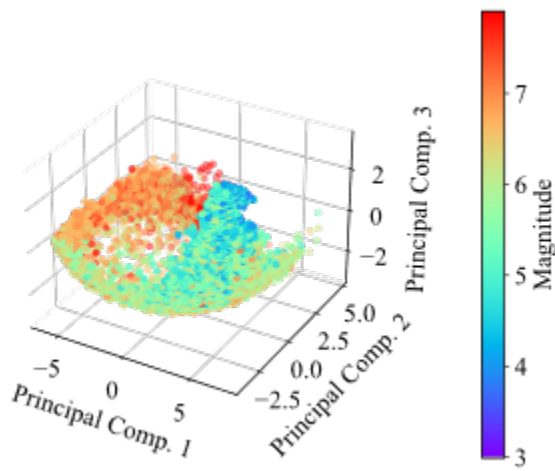
The final dataset includes ground-motion records with a complete range of magnitudes and energy contents downloaded from the PEER NGA-West 2 Database (Ancheta et al., 2013). Like the last example, the spline-based interpolation method resulted in a sequence length of

3981 for each spectrum, and filters were implemented to only include records with spectral data with a maximum acceleration above 0.01g. Training the network on a comprehensive group shows the pertinency of the framework to a large suite of ground motions, practical for real-world applications. In this example, there are no prior assumptions of a site, performance objectives, or intensity measures. However, design goals can be implemented by focusing the original dataset within the bounds a user defined seismic hazard analysis and used for the presented framework.

This set included 6,207 spectra. Matching the previous example, each record was encoded to 12 latent features. A PCA was conducted to linearly decompose the 12 latent features into the three features shown in the latent space representations in Figure 12. To deepen the understanding and interpretation of the latent space, multiple static IMs, or human engineered ground-motion measurements, are compared to the machine discovered latent features. This establishes the relationship with characteristics commonly understood in practice to the encoded attributes. Histograms show the distribution of the IMs among the original spectra. The reconstruction error and an example of an individual reconstruction is shown in Figure 13.

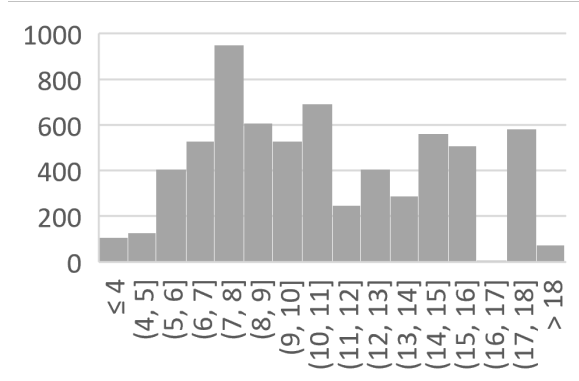
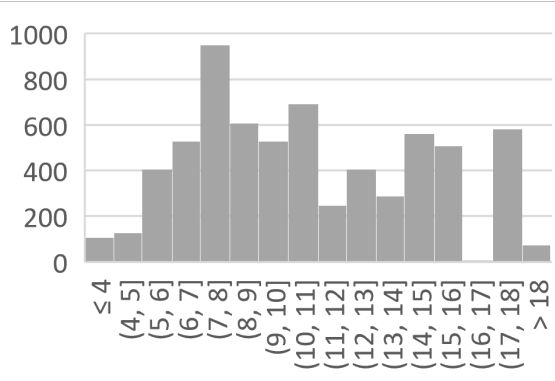
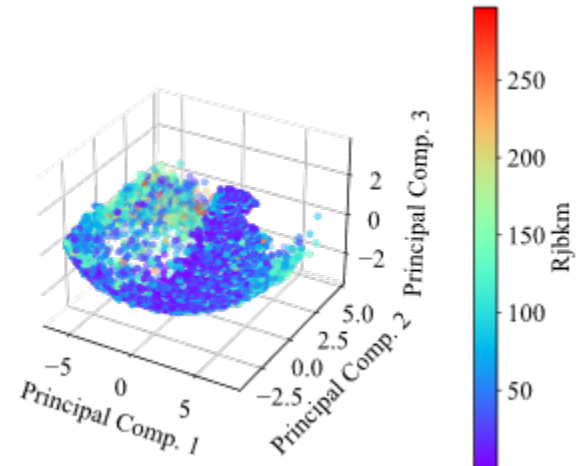
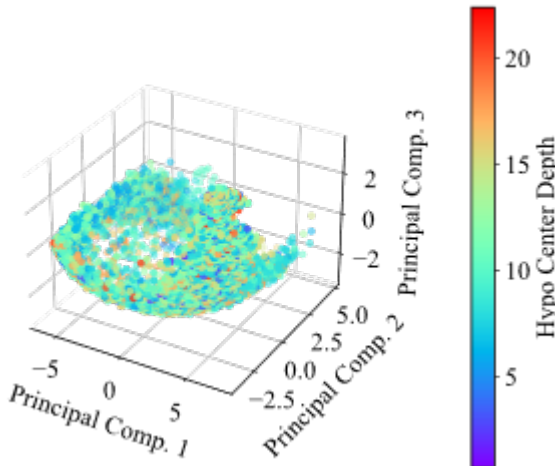
In practical applications, the desired number of clusters is not always explicitly identified with standard methods (e.g., the elbow method or silhouette method). One method of choosing the number of clusters could be to set the number of clusters to the number of desired spectra, limited by the availability of computational capacity for structural analysis or demands by engineering codes and standards. Multiple spectra could also be chosen from each cluster. For example, one selection could be the spectra closest to the centroidal spectra, and another selection could be the spectra furthest from the centroidal spectra. For this case, the latent space was separated into 5 clusters through k-means clustering in Figure 12 to align with Chapter 21 of ASCE 7 (ASCE 7-16: 2000). To further illustrate the clustering result, the scaled spectra is grouped by the assigned clusters from the latent space grouping presented in Figure 14. These images reveal a clear pattern between clustered spectra (e.g. spectral shape). Overall, ground-motion selection is accomplished with this framework through interpretable latent features and the flexibility to find clear cluster partitions in the source data.





(a)

(b)



(c)

(d)

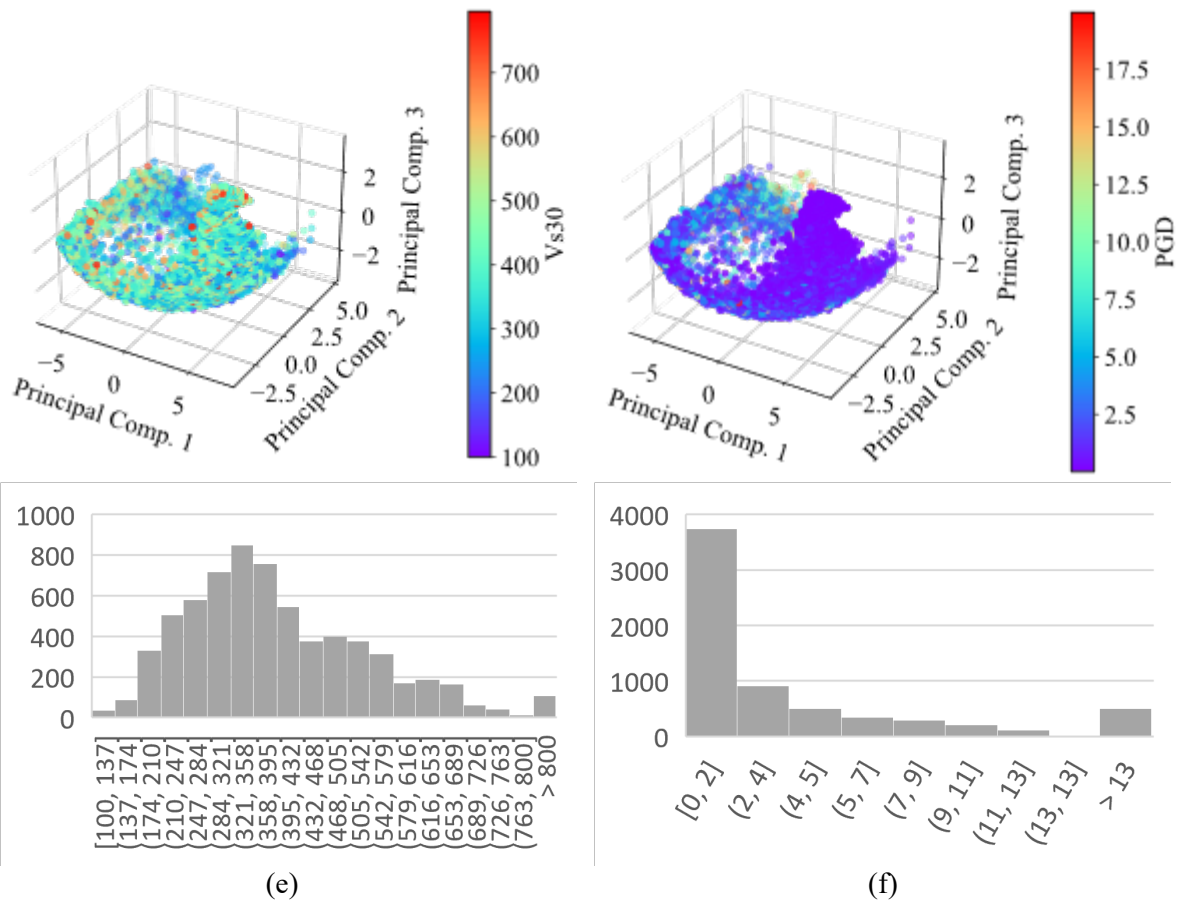


Figure 12: Latent space for comprehensive suite of ground motions colored by (a) the magnitude; (b) the fault rupture area; (c) the hypo center depth; (d) Joyner-Boore source-to-site distance ( $R_{j b k m}$ ); (e) shear wave velocity ( $V_{s30}$ ); (f) peak ground displacement (PGD).

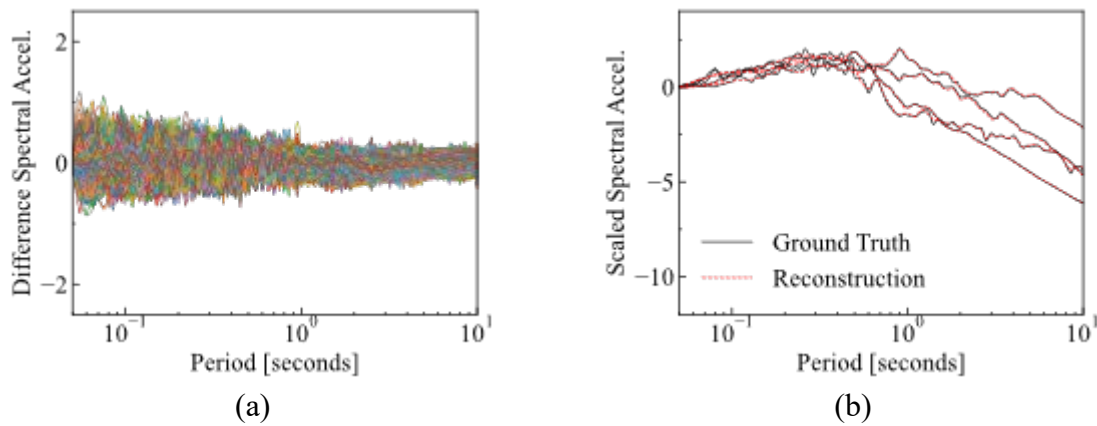


Figure 13: (a) Difference from input and reconstructed spectra; (b) reconstruction example.

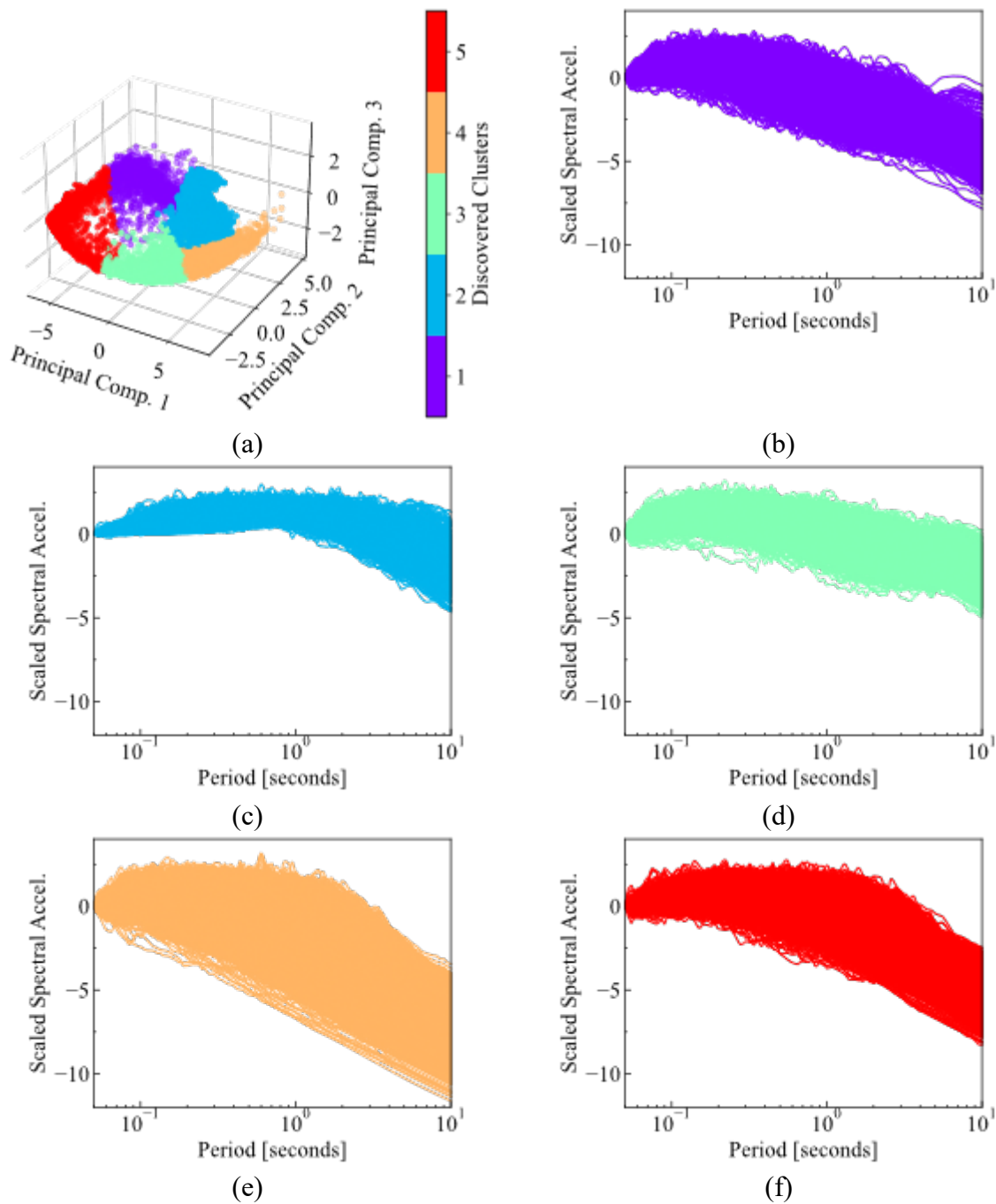


Figure 14: Clustering of scaled spectra through the proposed framework: (a) the deep embedding discovered clusters; and the scaled spectra for (b) cluster 1; (c) cluster 2; (d) cluster 3; (e) cluster 4; (f) cluster 5;

To deepen the understanding of the presented framework, an ablation study is presented showing the results of the deep embedding without the residual connection. Figure 15 (a) shows an abbreviated network architecture without the residual connection. Figure 15 (b) can be compared to Figure 2 (c) to show the training loss reduces by an order of magnitude of about 10 by including the residual connection. The difference from the reconstructed spectra to the

input spectra for each case can be deduced from Figure 15 (c) and Figure 13 (a). Finally, the latent space, without the residual connection and with poor reconstruction, is not well organized by the magnitude (shown in Figure 15 (d)). Thus, the inclusion of the residual connection drastically improves the reconstruction performance and organizes the latent feature space into a more interpretable structure.

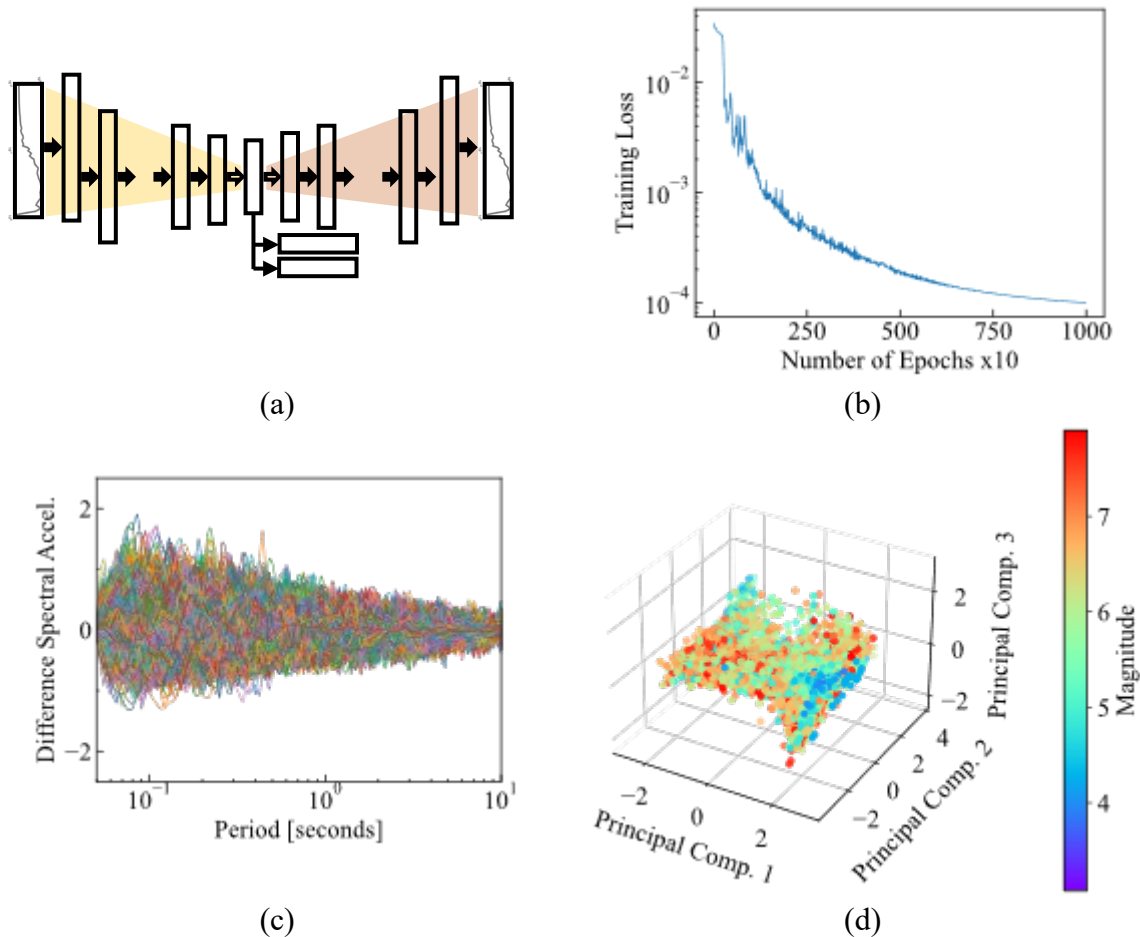


Figure 15: Ablation study depicting, (a) the network architecture; (b) the training loss; (c) the difference in reconstructed spectra to input spectra; and (d) the latent space.

## CONCLUSION

This paper presents a deep embedding unsupervised ML approach for ground-motion selection. The selection of ground-motion records has a significant role in surrogate meta-modeling of structural systems under earthquake hazards. The proposed framework can uncover latent characteristics of earthquake spectra to expand the overall representation during selection for nonlinear structural time-history analysis. This work utilized synthetic data and field ground-motion measurements to illustrate the effectiveness of the proposed framework.

The proposed framework particularly showed excellent clustering ability in the two validation examples, correctly clustering all 200 synthetic spectra by the original groups, and separating the field measured NGA spectra, grouped by magnitude, with 99% accuracy. In general, the framework can uncover latent attributes which maintain interpretable characteristics and are practical for clustering. Furthermore, the proposed approach is fundamental in nature and can be applied to cluster any type of sequential data in the time, frequency, and spectral domains.

## ACKNOWLEDGMENTS

We wish to acknowledge the support by the Engineering for Civil Infrastructure program at National Science Foundation under grant CMMI-2013067. We would also like to thank the reviewers for their role in improving our manuscript.

## DATA AVAILABILITY STATEMENT

All the source codes to reproduce the results in this study are available on GitHub at <https://github.com> (detailed URL will be provided after official publication of this paper).

## REFERENCES

- Ancheta, T., Darragh, R., Stewart, J., Seyhan, E., Silva, W., Chiou, B., Wooddell, K., et al., 2013. PEER NGA-West2 Database, Technical Report PEER 2013/03, (May 2013).
- ASCE 7-16: Minimum design loads for buildings and other structures*, 2000. *ANSI/ASCE Standard*. DOI: 10.1061/9780872629042
- Baker, J. W., 2011. Conditional mean spectrum: Tool for ground-motion selection. *Journal of Structural Engineering*, **137**(3), 322–331. DOI: 10.1061/(ASCE)ST.1943-541X.0000215
- Baker, J. W., and Cornell, C. A., 2006. Spectral shape, epsilon and record selection. *Earthquake Engineering and Structural Dynamics*, **35**(9), 1077–1095. DOI: 10.1002/eqe.571
- Baldi, P., 2012. Autoencoders, Unsupervised Learning, and Deep Architectures. *ICML Unsupervised and Transfer Learning*, 37–50. DOI: 10.1561/22000000006
- Bazzurro, P., and Luco, N., 2005. Do Scaled and Spectrum-Matched Near-Source Records

- Produce Biased Nonlinear Structural Responses. *National Conference on Earthquake Engineering* (Vol. 94111).
- Bengio, Y., Courville, A., and Vincent, P., 2013. *Representation Learning: A Review and New Perspectives*. *IEEE Transactions on Pattern Analysis and Machine Learning*. IEEE Computer Society. DOI: 10.1007/978-3-319-42471-2\_8
- Coates, A., and Ng, A. Y., 2012. *Learning Feature Representations with K-means*. (G. Montavon, G. B. Orr, and K. R. Müller, Eds.) *Neural Networks: Tricks of the Trade: Lecture notes in computer science* (Vol. 7700 LECTU).
- Ding, Y., Peng, Y., and LI, J., 2020. Cluster Analysis of Earthquake Ground-Motion Records and Characteristic Period of Seismic Response Spectrum. *Journal of Earthquake Engineering*, **24**(6), 1012–1033. Taylor & Francis. DOI: 10.1080/13632469.2018.1453420
- Grigoriu, M., 2011. To Scale or Not to Scale Seismic Ground-Acceleration Records. *Journal of Engineering Mechanics*, **137**(4), 284–293. DOI: 10.1061/(asce)em.1943-7889.0000226
- Hancock, J., Watson-Lamprey, J., Abrahamson, N. A., Bommer, J. J., Markatis, A., McCoyh, E., and Mendis, R., 2006. An improved method of matching response spectra of recorded earthquake ground motion using wavelets. *Journal of Earthquake Engineering*, **10**:S1, 67–89. DOI: 10.1080/13632460609350629
- Housner, G. W., and Jennings, P. C., 1982. *Earthquake design criteria*. Berkeley, CA: Earthquake Engineering Research Insitutue.
- Iervolino, I., Galasso, C., and Cosenza, E., 2010. REXEL: Computer aided record selection for code-based seismic structural analysis. *Bulletin of Earthquake Engineering*, **8**(2), 339–362. DOI: 10.1007/s10518-009-9146-1
- Katsanos, E. I., Sextos, A. G., and Manolis, G. D., 2010. Selection of earthquake ground motion records: A state-of-the-art review from a structural engineering perspective. *Soil Dynamics and Earthquake Engineering*, **30**(4), 157–169. Elsevier. DOI: 10.1016/j.soildyn.2009.10.005

- Kodinariya, T. M., and Makwana, P. R., 2013. Review on determining number of Cluster in K-Means Clustering. *International Journal of Advance Research in Computer Science and Management Studies*, **1**(6), 2321–7782.
- Kong, Q., Trugman, D. T., Ross, Z. E., Bianco, M. J., Meade, B. J., and Gerstoft, P., 2019. Machine learning in seismology: Turning data into insights. *Seismological Research Letters*, **90**(1), 3–14. DOI: 10.1785/0220180259
- Kramer, M. A., 1991. Nonlinear principal component analysis using autoassociative neural networks. *AIChE Journal*, **37**(2), 233–243. DOI: 10.1002/aic.690370209
- Lee, C.-Y., Xi, S., Gallagher, P. W., Zhang, Z., and Tu, Z., 1998. Deeply-Supervised Nets. *18th International Conference on Artificial Intelligence and Statistics (AISTATS)* (Vol. 3, pp. 1783–1786). San Diego, CA, USA.
- Lin, T., Haselon, C. B., and Baker, J. W., 2013. Conditional spectrum based ground motion selection. Part I: Hazard consistency for risk-based assessments. *Earthquake Engineering & Structural Dynamics*, **42**(12), 1847–1865.
- Long, W., Lu, Z., and Cui, L., 2019. Deep learning-based feature engineering for stock price movement prediction. *Knowledge-Based Systems*, **164**, 163–173. Elsevier B.V. DOI: 10.1016/j.knosys.2018.10.034
- Naeim, F., Alimoradi, A., and Pezeshk, S., 2004. Selection and scaling of ground motion time histories for structural design using genetic algorithms. *Earthquake Spectra*, **20**(2), 413–426. DOI: 10.1193/1.1719028
- Papazafeiropoulos, G., and Plevris, V., 2018. OpenSeismoMatlab: A new open-source software for strong ground motion data processing. *Heliyon*, **4**(9), e00784. Elsevier Ltd. DOI: 10.1016/j.heliyon.2018.e00784
- Pearson, K., 1901. On Lines and Planes of Closest Fit to Systems of Points in Space. *Philosophical Magazine*, **2**(11), 559–572. DOI: 10.1080/14786440109462720
- Pham, L., McLoughlin, I., Phan, H., Palaniappan, R., and Mertins, A., 2020. Deep Feature Embedding and Hierarchical Classification for Audio Scene Classification. *Proceedings*

of the International Joint Conference on Neural Networks. DOI: 10.1109/IJCNN48605.2020.9206866

Rehman, K., Burton, P. W., and Weatherill, G. A., 2014. K-means cluster analysis and seismicity partitioning for Pakistan. *Journal of Seismology*, **18**(3), 401–419. DOI: 10.1007/s10950-013-9415-y

Rowels, S. T., and Saul, L. K., 2000. Nonlinear dimensionality reduction by locally linear inlaying. *Science: New Series*, **209**(5500), 2323–2326. DOI: 10.1109/TNN.2008.2005582

Wang, H., Li, L., Chi, L., and Zhao, Z., 2019. Autism Screening Using Deep Embedding Representation. *Lecture Notes in Computer Science (including subseries Lecture Notes in Artificial Intelligence and Lecture Notes in Bioinformatics)*, **11537 LNCS**, 160–173. DOI: 10.1007/978-3-030-22741-8\_12

Whittaker, A. S., Atkinson, G. M., Baker, J. W., Bray, J. D., Grant, D. N., Hamburger, R., Haselton, C., et al., 2012. Selecting and Scaling Earthquake Ground Motions for Performing Analyses. *Proceedings of the 15th world conference on earthquake engineering* (pp. 4207–4217). Earthquake Engineering Research Institute.

Xie, J., Girshick, R., and Farhadi, A., 2016. Unsupervised deep embedding for clustering analysis. *33rd International Conference on Machine Learning, ICML 2016* (Vol. 1, pp. 740–749).

Yaghmaei-Sabegh, S., 2017. A novel approach for classification of earthquake ground-motion records. *Journal of Seismology*, **21**(4), 885–907. *Journal of Seismology*. DOI: 10.1007/s10950-017-9642-8

Zhang, R., Hajjar, J., and Sun, H., 2020. Machine Learning Approach for Sequence Clustering with Applications to Ground-Motion Selection. *Journal of Engineering Mechanics*, **146**(6), 04020040. DOI: 10.1061/(asce)em.1943-7889.0001766